A Comparative Study of the Seismic Response of Soil-Nailed Walls under the Effect of Near-fault and Far-fault Ground Motions

Maryam Mokhtari[*], Kazem Barkhordari, Saeed Abbasi Karafshani

Department of Civil Engineering, Faculty of Engineering, Yazd University, Yazd, Iran

Abstract

In recent years, with the growing use of the nailing method for stabilizing excavation walls, there has been a need for a comprehensive investigation of the behavior of this method. In the previous studies, the behavior of nailed walls has been investigated in static and dynamic states and under different conditions. However, due to the different feature of near-field ground motions, it is necessary to study the effect of these motions on the behavior of the nailed walls. Near-fault ground motion is significantly affected by the earthquake record direction and the rupture mechanism. So, in this study, to compare the effects of near-field and far-field ground motions, a two-dimensional (2D) soil- nailed wall was considered. PLAXIS 2D was used for the modeling of the soil-nailed wall system. An excavation with a dimension of 10 meters in height was taken into the account. In this study, 10 records (Five fault-normal near-field ground motion records and five far-field ground motion records), were recorded on the rock and applied to the model. These

[*]Corresponding author   mokhtari@yazd.ac.ir

ground motion records were derived from the near-fault ground motion record set used by Baker. These records were scaled to the Peak Ground Acceleration (PGA) of 0.35g and then applied to the bottom of the finite element models. Mohr-Coulomb model was then used to describe the soil behavior, and Elasto-plastic model was employed for the nails. A damping ratio of 0.05 was considered at the fundamental periods of the soil layer. The results showed that the generated values of bending moment, shear force and axial force in nails under the effect of the near-fault ground motions were more than those in the far-ault ground motions. These values were almost equal to 23% for the maximum bending moment, 30% for the shear force, and 22% for the axial force. The created displacement under the effect of near-fault ground motions was more than that in the far-fault since a higher energy was applied to the model in the near-field ground motions during a short time (pulse-like ground motions). In contrast, in the far-fault ground motions, due to the more uniform distribution of energy during the record, such pulse-like displacements were not observed in the system response. Increasing in nail length and soil densification, decreases the displacement of the soil-nailed wall but does not change the general behavior of the soil under the effect of near-field ground motions. Based on the obtained results, for a constant PGA, there were positive correlations between the values of the maximum displacement on the top of the wall and the PGV values of near-fault ground motion records. However, the mentioned correlations were not observed in the case of far-fault ground motions.

Introduction

In the last three decades, the use of reinforced soil has been increased. This wide use is due to its low price and simple implementation [1-6]. In some studies, it has been shown that the nailed walls have a better performance in comparison to gravity retaining walls [7, 8]. In the implementation of the nailing method and with the progress of excavation, the excavation wall tends to move inside, and steel elements prevent the excavation wall movement through the tensile force. Of course, to mobilize the tensile force in the steel elements, the movement of the wall is inevitable. The finite element method, rather than the limit equilibrium methods, has become a standard method to analyze the nailing walls, resulting in the accurate analysis of the walls' behavior [9]. During the last three decades, many case studies have been carried out; these include laboratory, numerical and analytical modeling of the behavior of the nailed walls, such as stability, wall displacement, displacement mode and force distribution, within nails in a static state. However, few investigations have been conducted on the dynamic behavior of such soil structures. As an example, Hang et al. (2005) implemented experiments using the shaking table test to study the effect of nail angle, nail length and vibration frequency on the seismic resistance and rupture mechanisms [10]. Sheikhbahaei et al. (2010) also investigated the dynamic performance of a nailed wall using a finite difference method. In this research, the effect of input exitation, nail angle, nail length and soil shear strength parameters on

the dynamic response of the nailed wall was investigated [11]. Wu et al. (2012) also indicated that the three-dimensional model considered for the dynamic and static analysis of nail-reinforcing slopes could well predict their behavior. The researchers used the finite element method in their modeling [12]. Jaya et al. (2013), investigating a nailed-wall model, also concluded that the maximum ground acceleration had the most effect on the wall dynamical behavior [13]. Further, Chavan et al. (2017) investigated slope stability using a nailing method. This study indicated that the contact between the nail and soil could play an important role in the dynamic response of the stabilized slopes. This contact exerts more force on the nails [14]. In addition, Yazdandoust (2017) investigated the effect of peak ground acceleration, loading time, and nail length on the dynamic response of a nailed wall using the shaking table test. He concluded that the nailed-wall response strongly depended on nail length and the input parameters. In this study, the effect of different parameters of excavation was also investigated [15].

Seismic motions recorded in the near-fault areas and the fault rupture direction are different from those observed in the far-fault areas [16]. Research has indicated that it is not possible to define a particular distance for near-field ground motions, but a distance of less than 20 km from the rupture and the earthquake epicentre is usually considered for the near-field records. [17, 18]. The records of near-field ground motions depend on the faulting direction and mechanism. The characteristics of these records include high

amplitude and a long period, peak ground velocity to peak groun acceleration ratio (PGV/PGA), peak ground displacement to peak ground acceleration ratio (PGD/PGA), and the presence of the bulk of energy in one or more pulses [19]. One of the most important properties of near-field ground motions is the directivity effect and the fling step [20]. The directivity effect depends on the rupture mechanism and propagation of the fault rupture, and the effect of the fling step is due to the permanent deformation caused by the fault rupture, creating the one-sided pulse of velocity. The directivity is either forward or backward. Generally, velocity pulses caused by the forward directivity phenomenon are two-sided. These two-sided velocity pulses, which are observed in the fault-normal component of near-field ground motions, are more destructive than the one-sided pulses caused by the fling step [21]. Some studies have also indicated that forward directivity is the most destructive cause in the structures influenced by the near-fault ground motions [20]. Unlike far-field ground motions, where ground motion energy is distributed throughout the vibration time, in these earthquakes, most of the ground motion energy is present in one or more of the first pulses. In this study, therefore, the effects of the frequency content of far-field and near-field ground motions on the dynamical response of a nailed wall were comparatively investigated. Accordingly, changes in parameters, such as wall displacement, maximum axial force, shear force and bending moment in nails, were investigated.

Numerical Modeling Steps

Figure (1) represents the considered model; it includes an excavation with the depth of 10 meters that is stabilized with nail-reinforcing method. The range and dimensions of the model were based on the previous studies [22]. The considered model was controlled with FHWA manual (FOS=1.7). The excavation height, which was carried out in 5 steps, was 10 meters. The length of nails was 7 meters and their placement angles were 15 degrees. The horizontal and vertical spacing of the nails was 1 meter. The dimensions of the model were selected in such a way that the boundaries would have the least effect on the results. Given the loading symmetry and geometry, half of the model was considered. The analyses were performed using the finite element method and the PLAXIS 2D software. In practice, nails were tightened to the shotcrete facing [23]. The PLAXIS 2D software uses plate elements to model nails and shotcrete. In these elements, rigid connections are used by default. A 15-node triangular element was used for meshing. The mesh size in this software ranges from very coarse to very fine. The characteristics of the assumed material for soil are given in Table (1). The Mohr-Coulomb behavioral model was also used to describe the soil behavior. In addition, the assumed properties of nails and the shotcrete are listed in tables (2) and (3), respectively. To describe these two parts, the elasto-plastic behavior of nails and the elastic behavior of the shotcrete were considered.
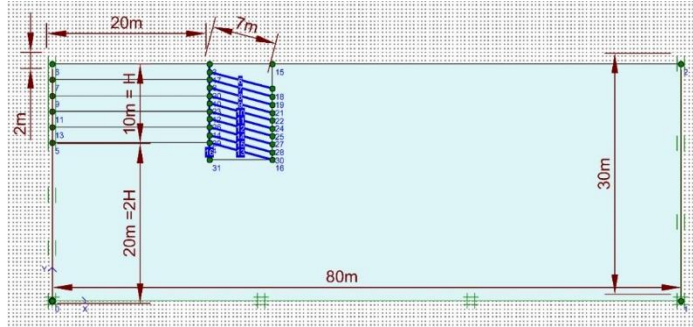
Figure 1. Dimensions and parts of the model

Table 1. Properties of the soil

Parameters	Symbol(unit)	Value
Unit weight	$\gamma(kN/m^3)$	19
Modulus of elasticity	$E(kN/m^2)$	35000
Poisson ratio	ν	0.3
Cohesion	$C(kPa)$	9
Friction angle	φ°	30
Dilatancy angle	ψ°	0

Table 2. Properties of nails

Parameters	Symbol(unit)	Value
Unit weight	$\gamma(kN/m^3)$	24
Elasticity modulus of nails	$E_n(GPa)$	200
Elasticity modulus of grout	$E_g(GPa)$	22
Poisson ratio	ν	0.2
Flexural stiffness	$EI(kNm^2/m)$	142.14
Axial stiffness	$EA(kN/m)$	228000
Maximum bending moment	$M_p(kNm/m)$	0.644
Maximum Axial force	$N_p(kN/m)$	216
Drill hole diameter	cm	10
Nail diameter	mm	25

Table 3. Properties of shotcrete

Parameters	Symbol (unit)	Value
Unit weight	$\gamma (kN/m^3)$	24
Elasticity modulus of	$E\,(GPa)$	220
Poisson ratio	V	0.2
Flexural stiffness	$EI\,(kNm^2/m)$	14670
Axial stiffness	$EA\,(kN/m)$	4400000
Shotcrete thickness	cm	20

Table 4. Properties of elements used in modelling

Parts	Number of nodes	Integration method	Number of elements
Soil	15	12 points	1125
Nail and shotcrete	5	4 points	9

    The interface between soil and nails was also considered to be rigid. Finally, in this study, to compare the results, all models were assumed to have the same geometry.Soils and nails were modeled as the plane strain. Two effective and important parameters of the materials in modeling include flexural stiffness (EI) and axial stiffness (EA). Since the section of the nails is a circle with horizontal spacing, equivalent flexural and axial stiffness was used in the plate elements (with rectangular surfaces) to take into account the 3-D effect on simplifying the plane strain behavior.

    This kind of modeling can accurately represent the actual behavior of the excavation under static and dynamic loads [24]. For nails, the elasticity modulus (E_g) is obtained as a combination of the elastic

stiffness of grout and bar as follows:

$$E_{eq} = E_n \left(\frac{A_n}{A}\right) + E_g \left(\frac{A_g}{A}\right) \tag{1}$$

where E_g is the grout elasticity modulus, and E_n is the elasticity modulus of nails. Other equations are as follows:

$$A = 0.25\pi D_{DH}^2 \tag{2}$$
$$A_n = 0.25\pi d^2 \tag{3}$$
$$A_g = A - A_n \tag{4}$$

where A is the total cross- sectional area of grouted soil nail; A_g is the cross- sectional area of grout cover; A_n is the cross- sectional area of reinforcement bar; $_{DDH}$ is the diameter of the drilled hole, and d is the bar diameter.

$$EA \left(\frac{kN}{m}\right) = \frac{E_{eq}}{S_h} \left(\frac{\pi D_{DH}^2}{4}\right) \tag{5}$$

$$EI \left(\frac{kNm^2}{m}\right) = \frac{E_{eq}}{S_h} \left(\frac{\pi D_{DH}^4}{64}\right) \tag{6}$$

where S_h is horizontal spacing of the nail. Two types of boundary conditions were used in modeling. The bottom of the model was considered as the bedrock and statically constrained on both x and y directions. For constraining the lateral boundaries to avoid propagating earthquake waves in the soil media, adsorbent boundaries were used. One of the essential parameters in dynamic analysis is damping ratio . The damping applied on the soil was considered as the Riley's damping. The damping matrix is a linear combination of the mass matrix and the initial stiffness, as follows:

$$[c] = \alpha[m] + \beta[k] \tag{7}$$

where α and β are the constant coefficients obtained from the following equations:

$$\alpha = \frac{2\xi\omega_1\omega_2}{\omega_1+\omega_2} \tag{8}$$

$$\beta = \frac{2\xi}{\omega_1+\omega_2} \tag{9}$$

where ω_2 and ω_1 refer to the angular frequency of the modes 1 and 2, which can be obtained using the modal analysis, ξ is critical damping, with the value of 0.05 [25]. With these conditions, α and β are 0.257 and 0.060, respectively.

In a study conducted by Baker [26], a set of near-field ground motion records were porposed, which had a pulse due to the forward directivity in the time history of ground motion velocity. Given the problem hypothesis that the location of the records was assumed on the bedrock, 10 records (five fault-normal near-field ground motion records and five far-field ground motion records) were obtained on the rock (by the records introduced by Baker) to conduct the analyses.The characteristics of these records are given in tables (5) and (6). To use these accelerograms, these records were scaled to the Peak Ground Acceleration (PGA) of 0.35 g. Figure (2) represents the Fourier spectrum of some selected accelerograms. Stage construction was used to solve the problem. In this case, it was possible to model each excavation step, nail placement and shotcrete implementation, separeately and in a step by step procedure. For this model, the entire executive process was performed in five steps. This method was implemented using the PLAXIS 2D software. After modeling the initial stages, the ground motion effect was applied on the bottom of the model (bedrock location).

Validation

To validate the model, the modeling implemented by Singh and Babu (2008) was used [27]. In this paper, a model with the depth of 8 meters, and the nails with the length of 4.7 meters and the diameter of 16 mm was considered for reinforcing the excavation wall. In Figure 3, the assumed model used for validating and comparing the numerical analysis results with those presented by Singh and Babu [27] is shown. Comparing the results obtained from the numerical analysis and those presented by Singh and Babu [27] are in good agreement with static and dynamic states.

Table 5. Selected near-fault ground motions

NO.	Earthquake	Year	Station	Tp(s)	PGA (g)	PGV (m/s)	Mw
1	San Fernando	1971	Pacoima Dam (upper left abut)	1.6	1.435	28	6.6
2	Coyote Lake	1979	Gilroy Array #6	1.2	0.452	4	5.7
3	Morgan Hill	1987	Coyote Lake Dam (southwest abut)	1	0.814	27	6.2
4	Cape Mendocino	1992	Petrolia	3	0.615	47	7
5	Northridge-01	1994	Pacoima Dam (downstream)	0.5	0.499	34	6.7

Table 6. Selected far-fault ground motions

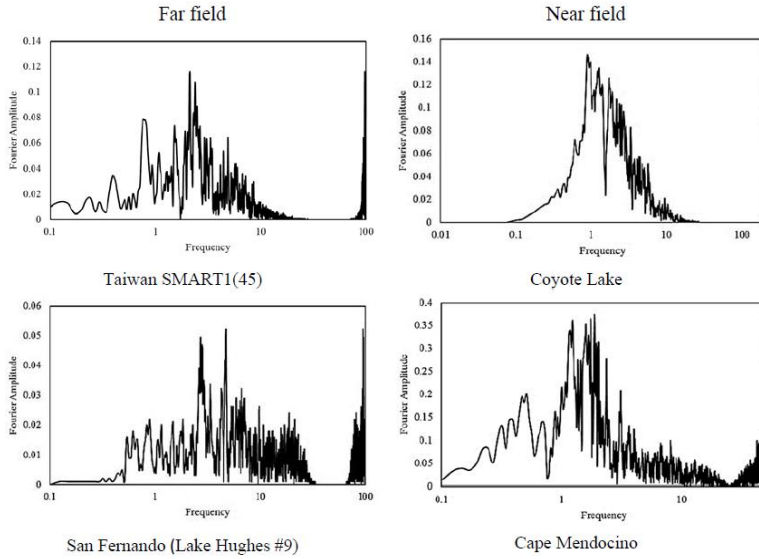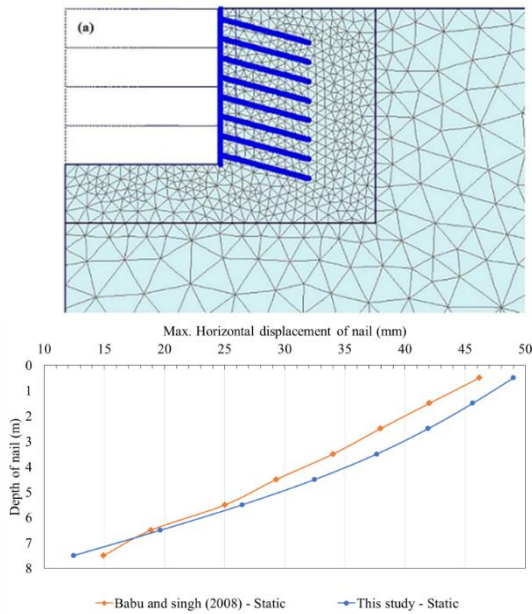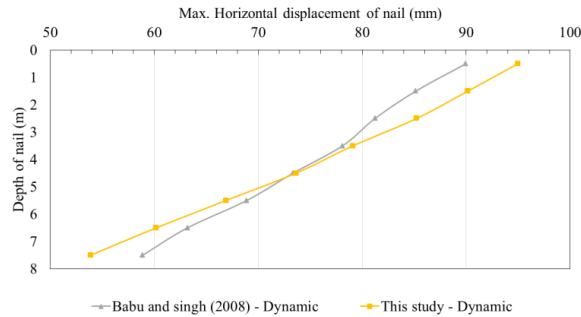| NO.	Earthquake	Year	Station	PGA (g)	PGV (m/s)	Mw
1	San Fernando	1971	Lake Hughes #9	0.17	10	6.6
2	San Fernando	1971	Santa Anita Dam	0.155	11	6.6
3	Irpinia, Italy-01	1980	Arienzo	0.31	2.73	6.9
4	Taiwan SMART1(45)	1986	SMART1 E02	0.136	36.7	7.3
5	Nahanni	1985	Site 1	0.94	15	6.76

Figure 2. Fourier spectrum for some records

(a)

(b)

Figure 3. (a) Model for validation and (b) Comparison of the obtained results

Results and Discussion

1. Investigating the Soil Behavior

Comparison of the results of near-field and far-field ground motions was used to present and analyse the results of this research. This method helped to simply analyse the results. The comparison of the spectrum of ground motion velocity and the relative displacement of the wall top under the influence of near-field and far-field ground motions is shown in Figure 4. As previously mentioned regarding the characteristics of the near-field ground motions, the spectrum of ground motion velocity in the near-field ground motion contains a pulse, which is also a distinguishing feature of near-field versus far-field ground motions. In figure 4 (b), the presence of a pulse in the spectrum of ground motion velocity under the Coyote Lake (near-field) and San Fernando (far-field) ground motions can be observed. As can be seen, there was a great velocity pulse in the spectrum of near-field ground motion velocity,

whereas this behavior was   not observed in the far-field ground motion. The Coyote Lake ground motion caused a pulse-like displacement in the wall. This pulse-like displacement is visible in Figure 4 (a). In all analyses, the peak ground acceleration was considered constant (equal to 0.35 g). Therefore, it could be said that this velocity pulse caused more displacement in the model under the effect of the near-field ground motions. On the contrary, in the far-field ground motions, displacement was uniformly applied during the ground motion period. As it can be seen in figure (5a), a residual displacement has been taken place at the end of analysis. Also, the residual displacement is larger in near-field ground motions. The main reason for large residual displacement in near-field ground motions is the existence of a pulse in these records that has let to change the soil behavior generally.
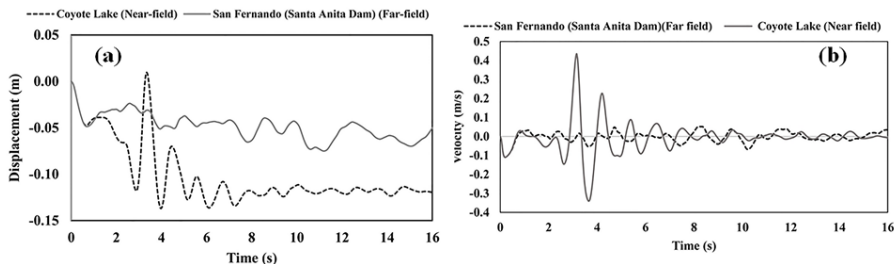

Figure 4. Comparison of (a) the maximum relative displacement of the top of the wall under the effect of near-fault and far-fault ground motions, and (b) Peak Ground Velocity at the surface of the earth
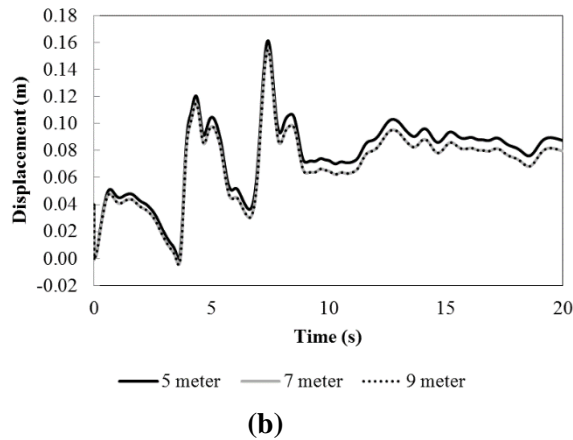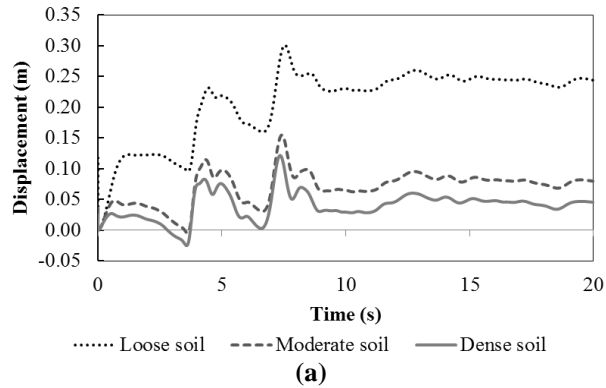
(a)

(b)

Figure 5. (a) Displacement of the top of the wall in the different soil conditions, (b) Displacement of the top of the wall in the different length of Nails

In order to cpmpare the effect of the near field and far field ground motions, two series of models were considered and analyzed. The displacement of the top of the wall in the different soil conditions are shown in figure (5a). Three conditions are considered for soil densification: (1) loose ($\gamma = 16\ kN/m^2\ \ , \varphi = 20°$), (2) moderate (($\gamma = 19\ kN/m^2\ \ , \varphi = 30°$) and (3) dense (($\gamma = 20\ kN/m^2\ \ , \varphi = 38°$). As it is demonstrated in figure 5 (a), the

displacement in loose soil is larger than moderate and dense soils. An important note in figure (5a) is that when the soil condition is changed, the behavior of soil under the effect of near-field ground motions has not been changed. It means that the general behavior of the soil is not dependent on the state of densification of soil but the amount of the displacement of the wall changens. Figure (5b) represents the displacement of the top of the wall varying by different nails length. In this figure the difference between the displacement of the wall for three lengths of nails (5, 7 and 9 meters) is shown. The results show that increase in nail length, consequences a decrese in the displacement of the wall. But, as mentioned in figure (5a), the general behavior of the soil was not changed with increase in the length of nails.

Figure 6 represents (a) the spectral acceleration response corresponding to the Coyote Lake record at the bedrock and ground surfaces, and (b) the spectral acceleration ratio at the soil surface to the spectral acceleration at the bedrock. It can be seen that the predominant period of soil changed as earthquake waves passed through the soil. To study the variations of the predominant period of a soil layer by applying a specific ground motion record in each period, the ratio of the pseudo-acceleration response spectral amplitude for the acceleration of a ground surface to the amplitude of the applied pseudo-accelerogram response spectrum was considered as a criterion to investigate these changes. By plotting the value of this ratio versus the period, a graph was obtained, where time

periods corresponding to its peaks indicated the variation of the soil period as a result of ground motion.

Figure (6b) represents this diagram for the Coyote Lake recoed. In this figure, the time period corresponding to the peak represents the time period of the soil layer in an almost linear state, and the longer time periods corresponding to the next peaks show an increase in the time period of the soil layer due to the nonlinear deformations. This behavior was observed in other near-field ground motions.
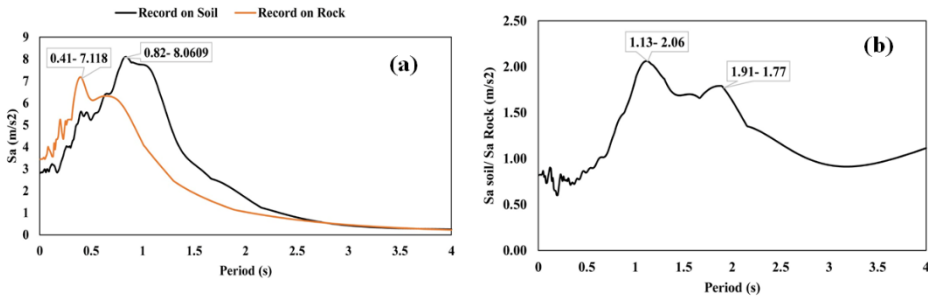

Figure 6. a) A spectral acceleration spectrum corresponding to the record of Lake Coyote at the bedrock and the surface of earth, and b) the ratio of the spectral acceleration at the soil surface to the spectral acceleration at the bedrock surface

A comparison of the model behavior under the ground motions (a) far-field (San Fernando (Santa Anita Dam)) and (b) near-field (Sano Fernando (Pacoima Dam (upper left abut)) is shown in Figure 7. This figure shows the acceleration spectrum, velocity and Arias intensity of the input excitation as well as displacement on the ground. It could be seen from the figure that there was no pulse in the acceleration spectrum of both near- and far-field ground motions. However, in the ground motion velocity spectrum, the presence of pulse in the

velocity spectrum of the near-field motion was clearly observable. In the next section of this figure, the graph related to the Arias intensity of the input excitation is shown. In all of these graphs, the effective duration of the earthquake (defined as the accumulation time of 5 to 85% of the Arias intensity) is shown for each excitation. As shown in the figure, this value for the near-field ground motion was 7.33 seconds, while for the far-field ground motion, it was equal to 11.31 seconds. Therefore, it could be said that in the near-field ground motion, more energy was exerted on the model in less time; in other words, the main energy of the near-field ground motions was exerted on the model within the pulse of their motions. Finally, the entire effect of this process on the displacement spectrum of the motions could be observed. In the near-field ground motion, the displacement in the model was pulse-shaped, generating a greater displacement in comparison to the far-field ground one . It seems that studying the effects of near-field earthquakes on structures can lead to remarkable changes in their design in the near-field regions

Figure 8 indicates the effect of the peak ground velocity on the maximum displacement of excavation under the effects of near-fault and far-fault ground motions. As can be seen, in a near-field ground motion and at a constant peak ground acceleration (PGA), the maximum excavation displacement was also increased with the rise of the peak ground velocity (PGV).
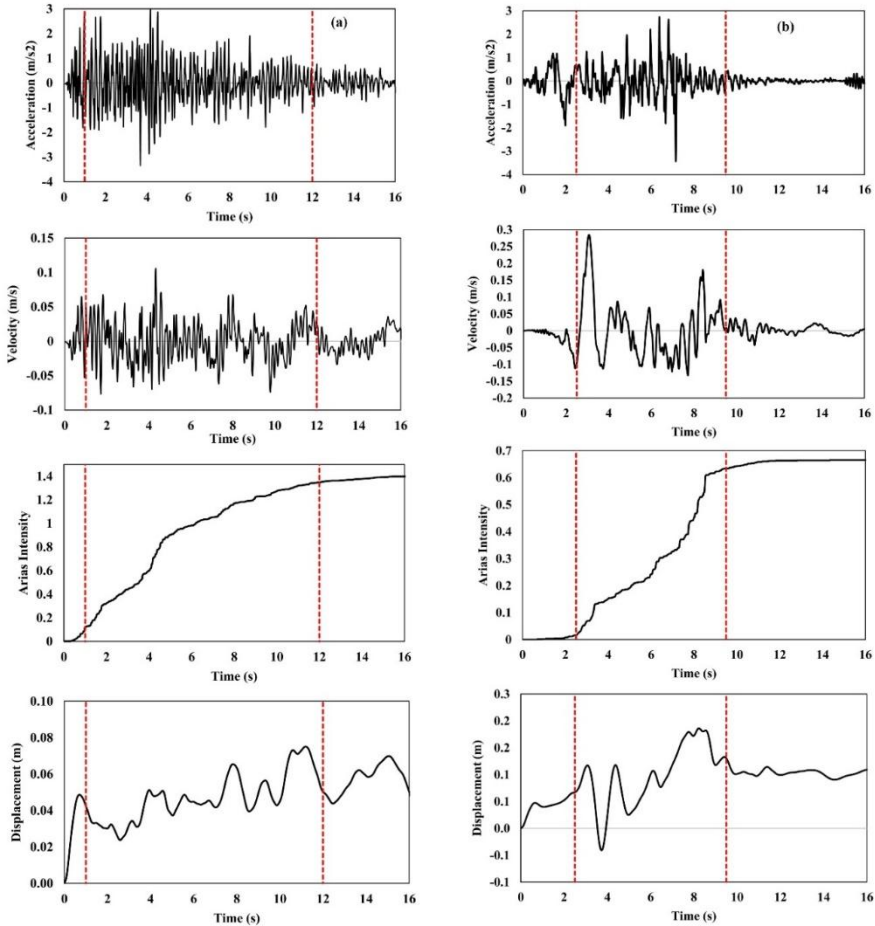
Figure 7. Comparison of the model response under the effect of (a) the near-fault ground motion (San Fernando (Pacoima Dam (upper left abut))) and (b) the far-fault ground motion (San Fernando (Santa Anita Dam))

However, there was no distinct correlation between the PGV value and excavation displacement in the far-fault ground motion. Generally, according to the results of the previous studies, many parameters can affect the excavation behavior under the effective

dynamic load. However, based on the graphs of Figure 8, PGV values are also one of the most effective parameters in the near-field ground motion (not mentioned in the previous studies), while this conclusion can not be valid in the far-field ground motions.
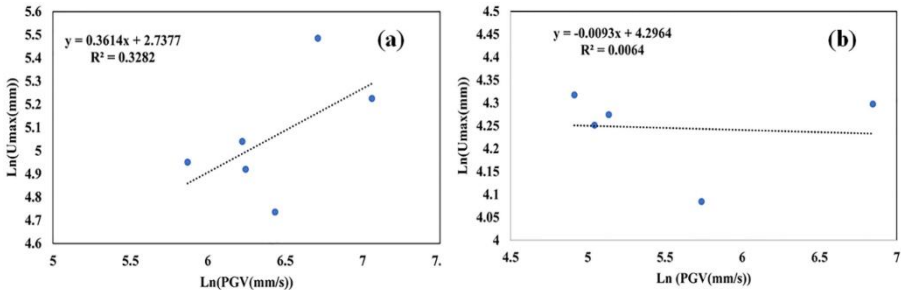

Figure 8. The effects of Peak Ground Velocity (PGV) on the maximum displacement of excavation under the effects of (a) near-fault and (b) far-fault ground motions

2. Investigating the nails behavior

Figure 9 represents the comparison between the logarithmic average of (a) the maximum bending moment, (b) the aximum shear force, and (c) the maximum axial force generated in the nails under near and far-field ground motions. It could be observed that the maximum values of the bending moment, the shear force and the axial force generated within the   nails in the near-field ground motions were higher than those generated under far-field ones in all three graphs.

These values were   almost equal to 23% for the maximum bending moment, 30% for the shear force, and 22% for the axial force. This indicated the importance of investigating the behavior of nailed walls under the influence of near-field ground motions. In

addition, special attention should be paid to designing nails in areas where the occurrence of near-field faults is possible.
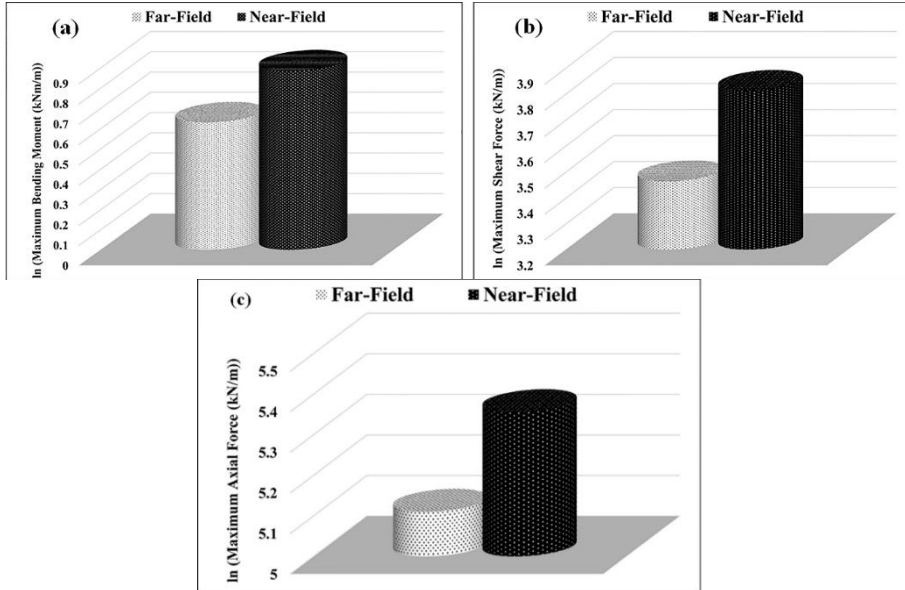

Figure 9. Comparison of the logarithmic averages of (a) bending moment, (b) shear force and (c) axial force in the nails under the effect of near-fault and far-fault ground motions

Conclusion

In this research, the effect of near-field and far-field ground motions on the response of the model was investigated by taking into account a two-dimensional (2-D) excavation model. the Mohr-Coulomb model and the elasto-plastic model utilized to describe the soil behavior and nails, respectively. In addition, by considering the features of the PLAXIS 2D software, we used the stage construction method to figure out the excavation modeling trend. In this study, 10 records were applied on the

bottom of the model and recorded on the hard rock (five near-field ground motion records and five far-field ground motion records). The obtained results were as follows:

• This study confirms that in the near-field ground motions, more energy was applied to the model in less time. The main energy of the near-field ground motions existed in the pulse of their motions.

• In the near-field ground motion, the displacement was a pulse-like shape in the model and was greater than that in the far-field ground motion.

• Increasing in nail length and soil densification, decrease the displacement of the soil-nailed wall but do not affect the general behavior of the soil under the near-field ground motions.

• In the near-field ground motions, in a constant peak ground acceleration (PGA), the maximum displacement of excavation was also enhanced with an increase in the peak ground velocity (PGV).

• The values of the bending moment, the shear force and the axial force generated within nails in the near-field ground motion were higher than those generated under the far-field ground motions. These values were almost equal to 23% for the maximum bending moment, 30% for the shear force, and 22% for the axial force.

References

1. Miyata Y., Bathurst R. J., Konami T., "Evaluation of two anchor plate

capacity models for MAW systems", Soils and Foundations, Vol. 51, No. 5 (2011) 885-895.

2. Leshchinsky D., Vahedifard F., Leshchinsky B. A., "Revisiting bearing capacity analysis of MSE walls", Geotextiles and Geomembranes, Vol. 34 (2012) 100-107.

3. Dash S. K., Bora M. C., "Improved performance of soft clay foundations using stone columns and geocell-sand mattress", Geotextiles and Geomembranes, Vol. 41(2013) 26-35.

4. Suksiripattanapong C., Horpibulsuk S., Chinkulkijniwat A., Chai J. C., "Pullout resistance of bearing reinforcement embedded in coarse-grained soils", Geotextiles and Geomembranes, Vol. 36 (2013) 44-54.

5. Naeini S., Gholampoor N., "Cyclic behaviour of dry silty sand reinforced with a geotextile", Geotextiles and Geomembranes, Vol. 42, No. 6 (2014) 611-619.

6. Biabani M. M., Indraratna B., "An evaluation of the interface behaviour of rail subballast stabilised with geogrids and geomembranes", Geotextiles and Geomembranes, Vol. 43, No. 3 (2015) 240-249.

7. Tatsuoka F., Tateyama M., Koseki J., Uchimura T., Geotextile-reinforced soil retaining wall and their seismic bahaviour. in Special Lecture, Proceeding of the 10th Asian Regional Conference on SMFE, Beijing. Location.

8. Collin J. G., Chouery-Curtis V. E., Berg R. R., "Field observations of reinforced soil structures under seismic loading", Earth Reinforcement Practice (Ochiai, Hayashi and Otani, Eds.), Balkema, Proc. Int. Symp. on Earth Reinforcement Practice, Fukuoka, Japan, Vol. 1 (1992) 223-228.

9. Griffiths D., Lane P., "Slope stability analysis by finite elements", Geotechnique, Vol. 49, No. 3 (1999) 387-403.

10. Hong Y. S., Chen R. H., Wu C.-S., Chen J. R., "Shaking table tests and stability analysis of steep nailed slopes", Canadian Geotechnical Journal, Vol. 42, No. 5 (2005) 1264-1279.

11. Sheikhbahaei A. M., Halabian A. M., Hashemolhosseini S. H., "Analysis of soil nailed walls under harmonic dynamic excitations using finite difference method". *In* Proceedings of the Fifth International Conference on Recent Advances in Geotechnical Earthquake Engineering and Soil Dynamics, San Diego, Calif, Volume: 5.59a (2010).

12. Wu J. C., Shi R., "Seismic Analysis of Soil Nailed Wall Using Finite Element Method", in Advanced Materials Research. Location: Trans Tech Publ. Vols. 535-537 (2012) 2027-2031.

13. Jaya V., Annie J., "An investigation on the dynamic behavior of soil nail walls", Journal of Civil Engineering and Science, Vol. 2, No. 4 (2013) 241-249.

14. Chavan D., Mondal G., Prashant A., "Seismic analysis of nailed soil slope considering interface effects", Soil Dynamics and Earthquake Engineering, Vol. 100 (2017) 480-491.

15. Yazdandoust M., "Experimental study on seismic response of soil-nailed walls with permanent facing", Soil Dynamics and Earthquake Engineering, Vol. 98 (2017) 101-119.

16. Chopra A. K., Chintanapakdee C., "Comparing response of SDF systems to near-fault and far-fault earthquake motions in the context of spectral regions", Earthquake Engineering & Structural Dynamics, Vol.

30, No. 12 (2001) 1769-1789.

17. Alavi B., Krawinkler H., 2001, "Effects of near-fault ground motions on frame structures", John A. Blume Earthquake Engineering Center, (2001).

18. Ambraseys N., Douglas J., "Near-field horizontal and vertical earthquake ground motions", Soil dynamics and earthquake engineering, Vol. 23, No.1 (2003) 1-18.

19. Moustafa A., Takewaki I., "Characterization and modeling of near-fault pulse-like strong ground motion via damage-based critical excitation method", Structural engineering & mechanics, Vol. 34, No. 6 (2010) 755-778.

20. Kalkan E., Kunnath S. K., "Effects of fling step and forward directivity on seismic response of buildings", Earthquake spectra, Vol. 22, No. 2 (2006) 367-390.

21. Tothong P. Cornell C. A., "Structural performance assessment under near-source pulse-like ground motions using advanced ground motion intensity measures", Earthquake Engineering & Structural Dynamics, Vol. 37, No. 7 (2008) 1013-1037.

22. Briaud J. L., Lim Y., "Soil-nailed wall under piled bridge abutment: simulation and guidelines", Journal of geotechnical and geoenvironmental engineering, Vol. 123, No. 11 (1997) 1043-1050.

23. Joshi B., "Behavior of calculated nail head strength in soil-nailed structures", Journal of geotechnical and geoenvironmental engineering, Vol. 129, No. 9 (2003), 819-828.

24. Singh V. P., Babu G. S., "2D numerical simulations of soil nail walls", Geotechnical and Geological Engineering, Vol. 28, No. 4 (2010) 299-

309.

25. Cakir T., Livaoglu R., "Fast practical analytical model for analysis of backfill-rectangular tank-fluid interaction systems", Soil Dynamics and Earthquake Engineering, Vol. 37 (2012) 24-37.

26. Baker J. W., "Quantitative classification of near-fault ground motions using wavelet analysis", Bulletin of the Seismological Society of America, Vol. 97, No. 5 (2007) 1486-1501.

27. Babu G. S., Singh V. P., "Numerical analysis of performance of soil nail walls in seismic conditions", ISET Journal of Earthquake Technology, Vol. 45, No. (1-2) (2008) 31-40.